Research Square

Preprints are preliminary reports that have not undergone peer review.
They should not be considered conclusive, used to inform clinical practice,
or referenced by the media as validated information.

On-Chip Liquid and Gas Flow Rate Sensing via Membrane Deformation and Bistability Probed by Microwave Resonators

Arda Secme
Bilkent University
Hadi Sedaghat Pisheh
Bilkent University
H. Dilara Uslu
Bilkent University
Uzay Tefek
Bilkent University
Berk Kucukoglu
Bilkent University
Ceren Alatas
Bilkent University
Mehmet Kelleci
Bilkent University
M. Selim Hanay (selimhanay@bilkent.edu.tr)
Bilkent University

Research Article

Keywords: Flow Rate Sensing, Microwave Sensors, Microfluidics, Membranes

Posted Date: November 15th, 2022

DOI: https://doi.org/10.21203/rs.3.rs-2260428/v1

License: This work is licensed under a Creative Commons Attribution 4.0 International License.
Read Full License

Abstract

Precise monitoring of fluid flow rates constitutes an integral problem in various lab-on-a-chip applications. While off-chip flow sensors are commonly used, new sensing mechanisms are being investigated to address the needs of increasingly complex lab-on-a-chip platforms which require local and non-intrusive flow rate sensing. In this regard, the deformability of microfluidic components has recently attracted attention as an on-chip sensing mechanism. To develop an on-chip flow rate sensor, here we utilized the mechanical deformations of a 220 nm thick Silicon Nitride membrane integrated with the microfluidic channel. Fluid flow induces deformations on the membrane, which is electronically probed by the changes in the capacitance and resonance frequency of an overlapping microwave resonator. By tracking the resonance frequency, both liquid and gas flows were probed with the same device architecture. For liquid flow experiments, a secondary sensing mechanism emerged when it was observed that steady liquid flow induces periodic deformations on the membrane. Here, the period of membrane deformation depends on the flow rate and can again be measured electronically by the microwave sensor. Flow rate measurements based on the deformation and instability of thin membranes demonstrate the transduction potential of microwave resonators for fluid-structure interactions at micro and nanoscales.

Introduction

Local flow rate measurements on different fluidic channels are needed for various microfluidic applications. With flow rate sensing, one can control nutrient and cell concentrations in microscale chambers,(Wu et al. 2008; Mehling and Tay 2014) modify cellular adhesion rates on a substrate,(Christ and Turner 2010) and sort particles of different sizes.(Zhou et al. 2019) In organ-on-a-chip systems, cells need to be supplied with an optimal flux of nutrients to maintain their vitality.(Harink et al. 2013) Furthermore, finely controlled doses of drugs should be administered to test the response of cells from tumor biopsies.(Stevens et al. 2016; Cetin et al. 2017) In digital microfluidics, droplets with well-controlled sizes and compositions can only be generated by an exquisite and local control of different flow rates.(Ward et al. 2005; Garstecki et al. 2006; Glawdel et al. 2012) In most biomedical reactors, syringe or peristaltic pumps are used to set the flow rates; however, these devices have inherent delays and fluctuations that negatively affect the controllability of platforms. Commercial flow sensors are readily available, but naturally they are not integrated at the chip scale, impeding their utility for local flow sensing. Robust on-chip flow sensors appear to be the most efficient solution for flow rate measurements for microchannels.

Many different mechanisms have been used to develop flow rate sensors for microfluidic applications(Nguyen 1997; Ejeian et al. 2019; Cavaniol et al. 2022) which are classified as active and passive sensors depending on whether the sensor supplies energy to the fluid.(Cavaniol et al. 2022) Active sensors, based on thermal conductivity and Coriolis force, constitute the majority of the commercial devices. Thermal flow sensors work by heating a region along the channel and the heat transfer rate induced by fluid motion.(Dijkstra et al. 2007; Kuo et al. 2012; Lin and Burns 2015; Baldwin et al. 2016; Kim et al. 2019)

Thermal flow sensors do not require any moving parts and are relatively easy to fabricate. However, their operation depends critically on the knowledge of the heat capacity of the fluid, and their accuracy is degraded when the composition of fluid is complex whereby unaccounted channels for heat transfer arise. This dependency could create problems for application where flow composition changes over time. Coriolis flowmeters work by detecting the force perpendicular to the flow direction through an oscillating channel.(Enoksson et al. 1997; Haneveld et al. 2010) The higher complexity and cost of these sensors are compensated by the larger dynamic ranges they provide. Small fluidic channel diameters and induced heat on the fluid are regarded as the main shortcomings of active flowmeters.

In passive flow sensing, capacitive sensors,(Oosterbroek et al. 1999; Temiz and Delamarche 2018; Wissman et al. 2019) and optical sensors based on microbubble image velocimetry,(Chen et al. 2019; Tang et al. 2019) microparticle velocimetry(Salipante et al. 2017) laser Doppler velocimetry,(Campagnolo et al. 2013; Stern et al. 2014) and optofluidics(Cheri et al. 2014) were reported. Regarding mechanical flow rate sensors, cantilevers(Gass et al. 1993; Wexler et al. 2013) and spring-like structures(Attia et al. 2009) were used to measure the drag force in microfluidics channels. A cantilever-based sensor with variable-sized holes was manufactured and flow rate changes were correlated with cantilever deflection.(Noeth et al. 2014) This sensor worked by passing the fluid through a perforated cantilever structure: the deflection of the cantilever was then used to quantify the flow rate. While this system achieved 1 nL/min sensitivity, the flow needs to pass through the perforated mechanical structure. Numerous types of electrical flow sensors operating in the radio frequency have been reported.(Zarifi et al. ; Maenhout et al. 2019; Węglarski et al. 2020) Recently, Zarifi et al.(Zarifi et al. 2018) have developed a non-contact flow rate sensor that exploits the deflection of a thin polydimethylsiloxane (PDMS) layer and measured this deflection using a microwave sensor placed in close proximity. This sensor has reached a sensitivity of 0.5 µL/min, however the relaxation timescale of the elastomeric PDMS layer resulted in long recovery times (several minutes).

In this work, we investigated the deformations of a 220 nm Silicon Nitride membrane forming part of a microfluidic channel to achieve flow rate sensing (Fig. 1a). We chose Silicon Nitride owing to its desirable mechanical qualities compared to elastomers such as PDMS; this way, we expected to build a robust yet compliant sensor. The ceramic nature of the membrane increases the sensor durability and enhances its mechanical qualities, such as the ability to measure either liquid or gas flow through the same microfluidic channel and reaching fast mechanical recovery rates. The deformations of the membrane are probed by microwave electrodes directly placed on the membrane as described below. The interaction of fluid flow with a membrane can result in nonlinear effects, such as oscillations under constant flow as reported optically in various systems before.(Lammerink et al. 1995; Gervais et al. 2006; Ducloux et al. 2007; Kim et al. 2012; Xia et al. 2012; Xia et al. 2014; Stoecklein and Di Carlo 2018; Battat et al. 2022) By using the microwave transducer, we observed pulsations of the thin membrane with a period determined by the flow rate. Thereby a secondary flow sensing mechanism was demonstrated by measuring the membrane pulsation periods.

Experiments

We fabricated flow sensors by fabricating a coplanar wave guide (CPW) microwave resonator overlapping with a 220 nm thick membrane (Fig. 1). The microwave resonator can be modeled as an RLC circuit where the capacitance is determined by the distance between the signal and ground electrodes. In the case of the CPW geometry used in this work, the gap between the signal and ground electrodes was 400 μm which narrows down to 20 μm on the membrane, defining an active sensing region which overlaps with the thin membrane (Fig. 1b). When fluid flow deforms the thin membrane, the distance between the two electrodes changes, which induces a change in the capacitance —and consequently the resonance frequency— of the microwave resonator. The changes in the resonance frequency can be tracked by a custom electronic circuit based on phase-locked loops.(Kelleci et al. 2018)

The experimental setup consisted of two major subsystems: a microfluidic flow controller and an electronic measurement system (Fig. 1). The chip was placed under a microscope stage to directly observe the mechanical deformations of the membrane. To fabricate the device (Fig. 1b), we began with a commercially available wafer, consisting of 500 μm Si substrate, a 2 μm SiO_2 middle layer and a 220 nm Silicon Nitride top layer. The topmost Silicon Nitride eventually formed the membrane of interest (Figure S1a). Photolithography was performed on the backside of the wafer to define an etch window. The window was etched via inductively coupled plasma (Figure S1b) and left overnight in KOH wet etching (Figure S1c). KOH etched through Si and SiO_2, and a 220 nm thick membrane formed on the front surface. Sensors with different membrane sizes were utilized to monitor fine and coarse flow rates. The typical dimensions for the fabricated membrane are approximately 600–1500 μm in length and 300–500 μm in width.

Gold paths for defining the CPW microwave resonator were patterned on the front side of the wafer. Photolithography was performed with a mask aligned with respect to the thin film membrane (Figure S1d). Then, a 100 nm gold layer was deposited to form the signal and ground electrodes (Figure S1e). Coplanar waveguide resonator was designed to have a 50 Ω impedance to match the impedance of the electronic measurement system.

To fabricate the microfluidic channel, a negative photoresist (SU-8, Sigma-Aldrich) was used to fabricate the molds. Cured PDMS (ratio 10:1) was poured onto these molds and left to bake at 80^{o}C. Micro-channels, typically having dimensions of 300 μm in width and 150 μm in depth, were peeled off from the mold. Through plasma cleaning process, the micro channels were bonded on top of the chip and aligned with the membrane and gold electrodes (Figure S1f).

DI water was driven by a controllable pressure pump (MFCS-EZ, Fluigent) and passed through a commercial, thermal flow sensor (FRP, Fluigent) before reaching the microfluidic channel on the chip. The commercial flow sensor has a 430 μm ID borosilicate capillary and measures the flow rate by combining two different temperature readings obtained from two different locations inside the capillary. In between these two temperature sensors, there is a micro heater, and the flow rate value is calculated by the

dissipation of the heat. The range of this commercial sensor, calibrated with water, is 0–120 µL/min, with an accuracy of 5% above 2.4 µL/min and a 0.12 µL/min deviation below 2.4 µL/min. PTFE tubes were used to deliver the DI water to the micro channel.

Data acquisition was conducted with a custom-built LabVIEW program where the electronic data and flow rate values from a commercial sensor were simultaneously recorded every 50 msec. To increase the sensitivity of the microwave sensor, we utilized a narrow-band detection scheme which was centered around the first resonance frequency of the CPW structure. Phase-sensitive detection was performed with a lock-in amplifier (Zurich Instruments, MFLI). Due to the upper frequency limitation of the lock-in amplifier, we constructed an external heterodyne circuitry(Ferrier et al. 2009; Nikolic-Jaric et al. 2009; Afshar et al. 2016) to continuously track the resonance frequency (Figure S2). With a phase-locked loop (PLL), the phase of the resonator was locked to 0 degrees with a PI controller.(Kelleci et al.) Any deviation from 0 degrees emerged as an error signal, updating the frequency of the signal generator. With this method, we could effectively keep track of the shifts in the resonance.

Experimental Results

Flow Rate Sensing by Membrane Deformation

In the first experiments, we measured the shift in the resonance frequency of the microwave sensor as a function of flow rate. We investigated the response of the device from the reset condition (where there was no fluid flow) to the target flow rate while monitoring the resonance frequency of the microwave sensor (Fig. 2). When the flow rate reached a target value, sharp upward shifts in the resonance were observed. Each of these shifts depended on the magnitude of the flow rate (Fig. 2b), indicating that the amount of frequency shift can be used as a sensing parameter for the target flow rate.

The baseline frequency fluctuations were about ~ 1 kHz, from which one can extrapolate a short-term sensitivity level of 0.5 µL/min. However, as shown with the error bars of Fig. 2b, repeating the experiment at the same flow rate resulted in a dispersion in the frequency shifts with a standard deviation of 5.5 kHz which was larger than the baseline frequency noise. The sensor demonstrated here exhibited a time resolution of only several seconds when the flow rate was increased stepwise (Fig. 2c-d). When the flow was stopped, we observed a downward frequency drift that lasts for approximately 50 seconds (Fig. 2a) however, additional flow rate measurements can still be conducted during recovery period either using successive frequency shifts (Figure S7) or by directly working with the phase shift of the resonator (as in Fig. 2c-d).

After liquid flow rate experiments, we switched to experiments with pressurized air. For the first air flow experiment, we used a membrane with dimensions of 1.7 mm length and 1 mm width within a channel width of 0.25 mm. The resonance frequency was approximately 2.55 GHz. We spanned the pressure from 20 mbar until 1000 mbar. We have seen an almost linear relationship for the higher-pressure value (Fig. 3a), however, at low pressures the trend deviated from the linear response slightly.

To work at higher air flow rates, another device was fabricated with an increased channel width of 1.3 mm (instead of 0.25 mm, in the previous device). The size of the membrane was 3 x 1 mm and the resonance frequency of the microwave sensor was approximately 2.08 GHz. A monotonically rising frequency response was again observed as the applied pressure increased (Fig. 3b). The experiment also demonstrated that the device with 220 nm Silicon nitride membrane could endure an applied pressure up to 4 bar (Supplementary Video 1 shows the membrane deformation as the pressure is suddenly switched between the reset condition and 4 bar applied pressure).

Flow Rate Sensing by Membrane Pulsation Period

The interaction of thin membranes with microfluidics channels can result in dynamical bistability: indeed, oscillations of a flexible membrane under a constant input flow as demonstrated in numerous earlier work.(Lammerink et al. 1995; Gervais et al. 2006; Ducloux et al. 2007; Kim et al. 2012; Xia et al. 2012; Xia et al. 2014; Stoecklein and Di Carlo 2018; Battat et al. 2022) In our experiments at constant liquid flows, we observed periodic deformations of the membrane under optical microscopy as shown in Fig. 4 and Supplementary Video 2. To electronically read out the periodic deformations, the microwave sensor on the thin membrane can be used again as an integrated transducer.

The period of the modulations depends on the fluid flow rate as illustrated in Fig. 5. The figure shows the relation between the phase response of the resonator and the effective flow rate. Commercial flow rate sensor was placed in the experimental setup (as in Fig. 1a) to set the flow rate at a constant value. In this way, the desired flow rate values were set within the limit of sensitivity of the flow meter.

In Fig. 5a, two different flow rates, 10 and 5 µL/min, were tested. For a given constant flow rate, the time between two consecutive pulses, called the pulse interval (Ti), remained constant. As the flow rate was set to a different constant value, the pulse interval changed as well. When the flow rate was set to 10 µL/min, pulse interval T_1 was approximately 7 seconds, whereas at a 5 µL/min flow rate, pulse interval T_2 increased to approximately 14 seconds. Small peaks in the flow rate (as measured by the commercial sensor) were observed after each pulsation (Fig. 5b). Since a deflected membrane results in an enlarged channel, the fluidic resistance decreases which in turn results in a temporary increase in the flow rate.

We note that the experiments were conducted without using any components with cyclical mechanisms such as syringe pumps: rather, the flow was induced by pressure driven sources. We also conducted control experiments where commercial flow rate sensor was removed from the system and the fluid flow was provided through a vial kept at constant pressure. In this case, where only a constant pressure source drives the flow, we verified that membrane pulsations still occur (SI Table 1).

After the initial observations, we used three different device geometries to span different flow rates. To enhance the sensitivity of the resonator, a large membrane (1.5 mm x 0.3 mm) was fabricated and used to resolve the slight increments in the flow rate. The resonance frequency of the microwave sensor coupled to the first membrane was 3.66 GHz. As shown in Fig. 6 (blue data points), the flow rate was set to an interval of 0–1 µL/min with an incremental change of 0.1 µL/min via the reference sensor. Until 0.3

μL/min, the device did not register any pulsation in the resonance frequency. After reaching a flow rate of 0.4 μL/min, the device began to exhibit discernible pulses. Then, the flow rate increment was changed to 0.5 μL/min and a range of flow rate values were tested until 3.5 μL/min. Blue data points in Fig. 6 indicate an increasing relation between the flow rand the frequency of the pulsation.

A second device — with membrane dimensions of 0.8 mm by 0.35 mm, and a microwave resonance frequency of 2.36 GHz — was used to span a higher flow rate range. We started from 5 μL/min and recorded pulses for 300 seconds at each flow rate value. Then, the flow rate was increased with 5 μL/min steps, reaching a flow rate of 50 μL/min (red data points, Fig. 6). A third device — with membrane dimensions of 3 x 1 mm, and a microwave resonance frequency of 2.08 GHz — was used to operate at higher flow rates. This device could accommodate higher flow rates, since the width of the microfluidic channel was relatively large. Starting with 24 μL/min, we increased the flow rate until 120 μL/min which is the upper limitation of the commercial flow sensor. We kept observing a similar trend whereby the pulsation frequency correlates with the fluid flow rate (green data points, Fig. 6).

These results indicate that membrane-integrated microwave sensors can also be used for flow sensing by detecting the period of membrane oscillations. While at high flow rates, the observed pulsations occur frequently resulting in rapid update times for flow monitoring; at low flow rates, the duration between the pulses gets longer. As a result, the update rate of the device is slow for low flow rates, which constitutes a shortcoming of this secondary flow sensing mechanism.

Conclusion

In conclusion, we demonstrated that thin membranes integrated with microwave resonators can detect flow rates of fluids. Fluid flow induces deformations on the membrane, which in turn, modulates the capacitance of a microwave resonator. The capacitance change can be readily measured by tracking the resonance frequency of the microwave resonator. The choice of a sturdy Silicon Nitride membrane as the compliant mechanism enables the measurements of both liquid and gas flow through the same microfluidic architecture. In terms of mechanical transduction of liquid flow, in addition to the expected quasi-static deformation of the membrane, a secondary flowrate sensing mechanism emerges whereby steady flow induces periodic pulsations on the thin membrane. The pulsation period of the membrane can be sensitively measured by the changes of the phase response of the microwave sensor. For both sensing mechanisms, the high sensitivity of microwave resonators serves as a potent transducer for probing the interaction dynamics of fluid flow and thin membranes.

Declarations

ASSOCIATED CONTENT

Supporting Information

A Supplementary Information document containing further details and data about measurements is available. Two supplementary videos combining the fluorescent microscopy experiment is also provided.

ACKNOWLEDGMENT

The authors thank John E. Sader and Jesse Collis for helpful discussions. This project has received funding from the European Research Council (ERC) under the European Union's Horizon 2020 research and innovation program (grant agreement No 758769).

References

1. Afshar, S.,Salimi, E.,Braasch, K.,Butler, M.,Thomson, D. J.,Bridges, G. E.(2016). Multi-frequency DEP cytometer employing a microwave sensor for dielectric analysis of single cells, IEEE Transactions on Microwave Theory and Techniques; 64/3/991–998.
2. Attia, R.,Pregibon, D. C.,Doyle, P. S.,Viovy, J.-L.,Bartolo, D.(2009). Soft microflow sensors, Lab on a Chip; 9/9/1213–1218.
3. Baldwin, A.,Yu, L.,Meng, E.(2016). An electrochemical impedance-based thermal flow sensor for physiological fluids, Journal of Microelectromechanical Systems; 25/6/1015–1024.
4. Battat, S.,Weitz, D. A.,Whitesides, G. M.(2022). Nonlinear phenomena in microfluidics, Chemical Reviews; 122/7/6921–6937.
5. Campagnolo, L.,Nikolić, M.,Perchoux, J.,Lim, Y. L.,Bertling, K.,Loubiere, K.,Prat, L.,Rakić, A. D.,Bosch, T.(2013). Flow profile measurement in microchannel using the optical feedback interferometry sensing technique, Microfluidics and Nanofluidics; 14/1–2/113–119.
6. Cavaniol, C.,Cesar, W.,Descroix, S.,Viovy, J.-L.(2022). Flowmetering for microfluidics, Lab on a Chip;
7. Cetin, A. E.,Stevens, M. M.,Calistri, N. L.,Fulciniti, M.,Olcum, S.,Kimmerling, R. J.,Munshi, N. C.,Manalis, S. R.(2017). Determining therapeutic susceptibility in multiple myeloma by single-cell mass accumulation, Nature Communications; 8/1/1613.
8. Chen, Z.,Guo, Z.,Mu, X.,Li, Q.,Wu, X.,Fu, H.(2019). Packaged microbubble resonator optofluidic flow rate sensor based on Bernoulli Effect, Optics Express; 27/25/36932–36940.
9. Cheri, M. S.,Latifi, H.,Sadeghi, J.,Moghaddam, M. S.,Shahraki, H.,Hajghassem, H.(2014). Real-time measurement of flow rate in microfluidic devices using a cantilever-based optofluidic sensor, Analyst; 139/2/431–438.
10. Christ, K. V.,Turner, K. T.(2010). Methods to measure the strength of cell adhesion to substrates, Journal of Adhesion Science and Technology; 24/13–14/2027–2058.
11. Ducloux, O.,Talbi, A.,Gimeno, L.,Viard, R.,Pernod, P.,Preobrazhensky, V.,Merlen, A.(2007). Self-oscillation mode due to fluid-structure interaction in a micromechanical valve, Applied Physics Letters; 91/3/034101.
12. Ejeian, F.,Azadi, S.,Razmjou, A.,Orooji, Y.,Kottapalli, A.,Warkiani, M. E.,Asadnia, M.(2019). Design and applications of MEMS flow sensors: A review, Sensors and Actuators A: Physical; 295/483–502.

13. Enoksson, P.,Stemme, G.,Stemme, E.(1997). A silicon resonant sensor structure for Coriolis mass-flow measurements, Journal of microelectromechanical systems; 6/2/119–125.
14. Ferrier, G. A.,Romanuik, S. F.,Thomson, D. J.,Bridges, G. E.,Freeman, M. R.(2009). A microwave interferometric system for simultaneous actuation and detection of single biological cells, Lab on a Chip; 9/23/3406–3412.
15. Garstecki, P.,Fuerstman, M. J.,Stone, H. A.,Whitesides, G. M.(2006). Formation of droplets and bubbles in a microfluidic T-junction—scaling and mechanism of break-up, Lab on a Chip; 6/3/437–446.
16. Gervais, T.,El-Ali, J.,Günther, A.,Jensen, K. F.(2006). Flow-induced deformation of shallow microfluidic channels, Lab on a Chip; 6/4/500–507.
17. Glawdel, T.,Elbuken, C.,Ren, C. L.(2012). Droplet formation in microfluidic T-junction generators operating in the transitional regime. I. Experimental observations, Physical Review E; 85/1/016322.
18. Haneveld, J.,Lammerink, T. S.,de Boer, M. J.,Sanders, R. G.,Mehendale, A.,Lötters, J. C.,Dijkstra, M.,Wiegerink, R. J.(2010). Modeling, design, fabrication and characterization of a micro Coriolis mass flow sensor, Journal of micromechanics and microengineering; 20/12/125001.
19. Harink, B.,Le Gac, S.,Truckenmüller, R.,van Blitterswijk, C.,Habibovic, P.(2013). Regeneration-on-a-chip? The perspectives on use of microfluidics in regenerative medicine, Lab on a Chip; 13/18/3512–3528.
20. Kelleci, M.,Aydogmus, H.,Aslanbas, L.,Erbil, S. O.,Hanay, M. S.(2018). Towards microwave imaging of cells, Lab on a Chip; 18/3/463–472.
21. Kim, J.,Cho, H.,Han, S.-I.,Han, A.,Han, K.-H.(2019). A disposable microfluidic flow sensor with a reusable sensing substrate, Sensors and Actuators B: Chemical; 288/147–154.
22. Kim, S.-J.,Yokokawa, R.,Lesher-Perez, S. C.,Takayama, S.(2012). Constant flow-driven microfluidic oscillator for different duty cycles, Analytical Chemistry; 84/2/1152–1156.
23. Kuo, J. T.,Yu, L.,Meng, E.(2012). Micromachined thermal flow sensors—A review, Micromachines; 3/3/550–573.
24. Lin, W.-C.,Burns, M. A.(2015). Low-power micro-fabricated liquid flow-rate sensor, Analytical Methods; 7/9/3981–3987.
25. Mehling, M.,Tay, S.(2014). Microfluidic cell culture, Current Opinion in Biotechnology; 25/95–102.
26. Nguyen, N.(1997). Micromachined flow sensors—A review, Flow measurement and Instrumentation; 8/1/7–16.
27. Nikolic-Jaric, M.,Romanuik, S.,Ferrier, G.,Bridges, G.,Butler, M.,Sunley, K.,Thomson, D.,Freeman, M.(2009). Microwave frequency sensor for detection of biological cells in microfluidic channels, Biomicrofluidics; 3/3/034103.
28. Noeth, N.,Keller, S. S.,Boisen, A.(2014). Integrated cantilever-based flow sensors with tunable sensitivity for in-line monitoring of flow fluctuations in microfluidic systems, Sensors; 14/1/229–244.

29. Oosterbroek, R.,Lammerink, T. S.,Berenschot, J. W.,Krijnen, G. J.,Elwenspoek, M. C.,van den Berg, A. (1999). A micromachined pressure/flow-sensor, Sensors and Actuators A: Physical; 77/3/167–177.
30. Salipante, P.,Hudson, S. D.,Schmidt, J. W.,Wright, J. D.(2017). Microparticle tracking velocimetry as a tool for microfluidic flow measurements, Experiments in Fluids; 58/7/85.
31. Stern, L.,Bakal, A.,Tzur, M.,Veinguer, M.,Mazurski, N.,Cohen, N.,Levy, U.(2014). Doppler-based flow rate sensing in microfluidic channels, Sensors; 14/9/16799–16807.
32. Stevens, M. M.,Maire, C. L.,Chou, N.,Murakami, M. A.,Knoff, D. S.,Kikuchi, Y.,Kimmerling, R. J.,Liu, H.,Haidar, S.,Calistri, N. L.(2016). Drug sensitivity of single cancer cells is predicted by changes in mass accumulation rate, Nature Biotechnology; 34/11/1161–1167.
33. Stoecklein, D.,Di Carlo, D.(2018). Nonlinear microfluidics, Analytical chemistry; 91/1/296–314.
34. Tang, M.,Liu, F.,Lei, J.,Ai, Z.,Hong, S.-L.,Zhang, N.,Liu, K.(2019). Simple and convenient microfluidic flow rate measurement based on microbubble image velocimetry, Microfluidics and Nanofluidics; 23/11/118.
35. Temiz, Y.,Delamarche, E.(2018). Sub-nanoliter, real-time flow monitoring in microfluidic chips using a portable device and smartphone, Scientific Reports; 8/1/1–11.
36. Ward, T.,Faivre, M.,Abkarian, M.,Stone, H. A.(2005). Microfluidic flow focusing: Drop size and scaling in pressure versus flow-rate-driven pumping, Electrophoresis; 26/19/3716–3724.
37. Węglarski, M.,Jankowski-Mihułowicz, P.,Pitera, G.,Jurków, D.,Dorczyński, M.(2020). LTCC Flow Sensor with RFID Interface, Sensors; 20/1/268.
38. Wexler, J. S.,Trinh, P. H.,Berthet, H.,Quennouz, N.,Du Roure, O.,Huppert, H. E.,Lindner, A.,Stone, H. A. (2013). Bending of elastic fibres in viscous flows: the influence of confinement, Journal of fluid mechanics; 720/517–544.
39. Wissman, J. P.,Sampath, K.,Freeman, S. E.,Rohde, C. A.(2019). Capacitive bio-inspired flow sensing cupula, Sensors; 19/11/2639.
40. Wu, L. Y.,Di Carlo, D.,Lee, L. P.(2008). Microfluidic self-assembly of tumor spheroids for anticancer drug discovery, Biomedical Microdevices; 10/2/197–202.
41. Xia, H.,Wang, Z.,Fan, W.,Wijaya, A.,Wang, W.,Wang, Z.(2012). Converting steady laminar flow to oscillatory flow through a hydroelasticity approach at microscales, Lab on a Chip; 12/1/60–64.
42. Xia, H.,Wang, Z.,Nguyen, V.,Ng, S.,Wang, W.,Leong, F.,Le, D.(2014). Analyzing the transition pressure and viscosity limit of a hydroelastic microfluidic oscillator, Applied Physics Letters; 104/2/024101.
43. Zarifi, M. H.,Sadabadi, H.,Hejazi, S. H.,Daneshmand, M.,Sanati-Nezhad, A.(2018). Noncontact and nonintrusive microwave-microfluidic flow sensor for energy and biomedical engineering, Scientific Reports; 8/1/1–10.
44. Zhou, J.,Mukherjee, P.,Gao, H.,Luan, Q.,Papautsky, I.(2019). Label-free microfluidic sorting of microparticles, APL Bioengineering; 3/4/041504.

Figures

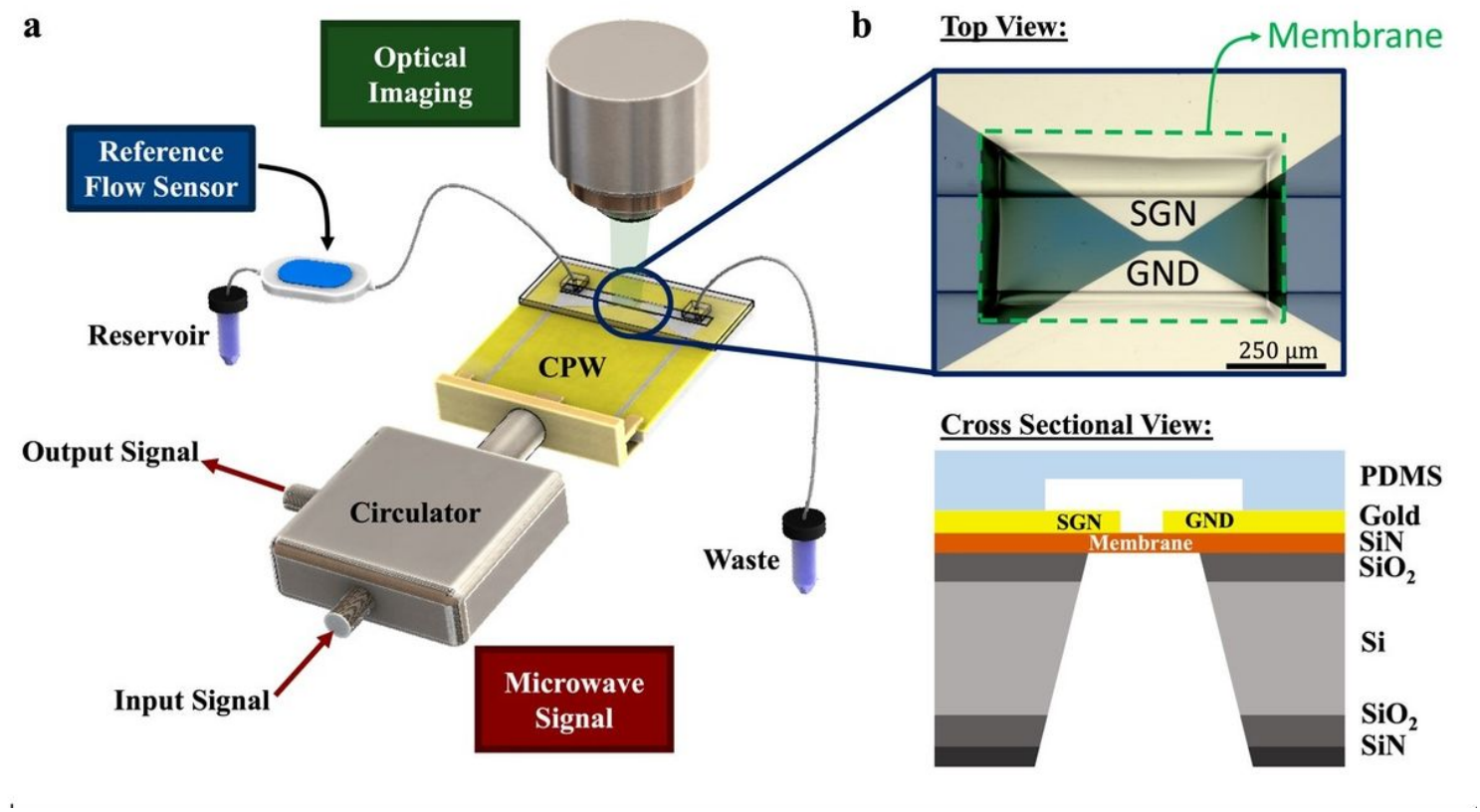

Figure 1

Experimental Configuration. (a) The chip was placed under a microscope to observe membrane deflections. Microfluidic tubing was connected first to a reference flow sensor, and then to the inlet port of the device. A circulator was employed to keep the single port microwave resonator at its resonance frequency. CPW: coplanar waveguide microwave resonator (b) Top view of the membrane taken under an optical microscope and cross-sectional schematics (not-to-scale) of the fabricated device. The membrane was suspended through wet etching, and then gold electrodes were fabricated in alignment with the membrane to form part of the microwave resonator. The signal (SGN) and ground (GND) electrodes of the microwave resonator extend towards each other and overlap with the membrane for capacitive detection of deformation. The PDMS microchannel was positioned manually on top of the gold electrodes and membrane.

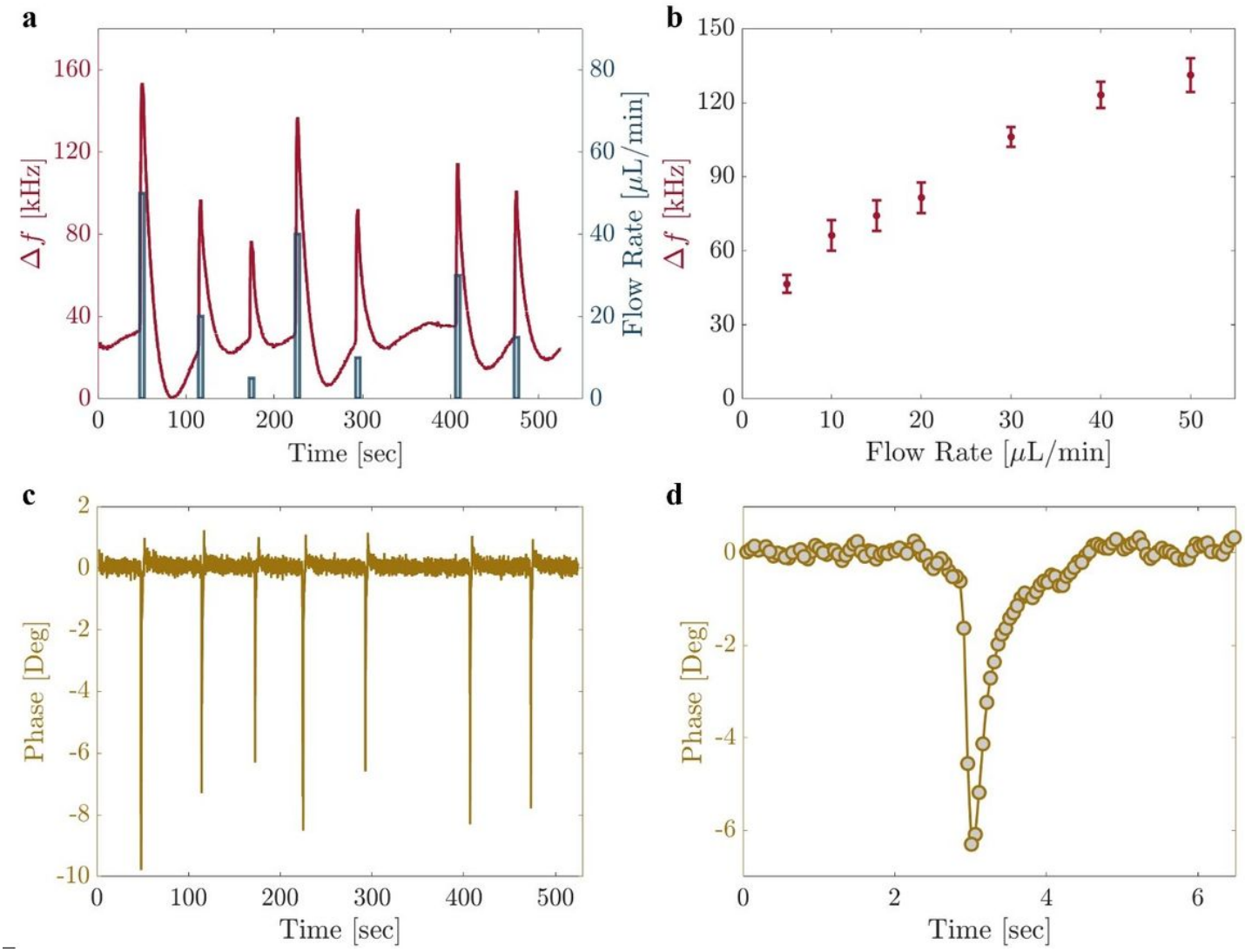

Figure 2

(a) Frequency response of the device from the reset fluid flow. (b) Frequency shifts *versus* the target flow rate. The shifts show a monotonically increasing behaviour. (c) Phase response of the data depicted in (a) from the reset fluid flow condition. (d) Close-up view shows fast settling time for phase response.

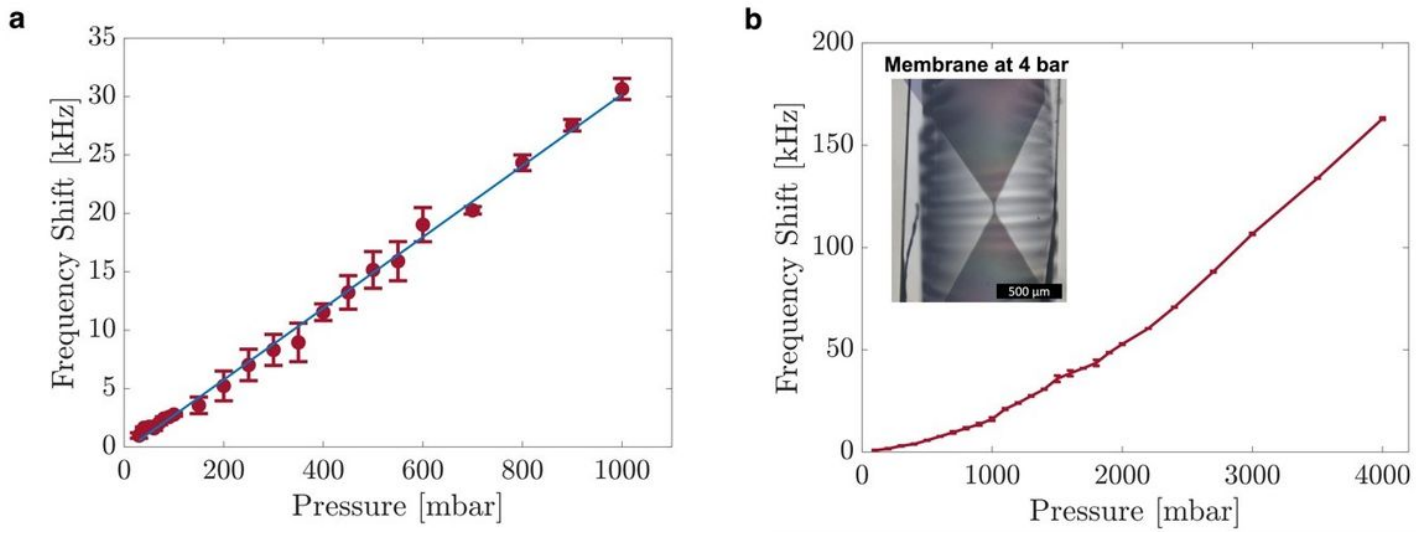

Figure 3

Frequency response of the device from the reset fluid flow of gas. (a) The response of the membrane with 1.7 mm x 1 mm in size coupled to a channel of 0.25 mm width. (b) The response of the membrane with 3 mm x 1 mm in size coupled to a channel of 1.3 mm width. The pressure was increased up to 4 bar and a monotonically increasing response is observed. Inset show the micrograph of the membrane and the channel when the gas inlet pressure is at 4 bar.

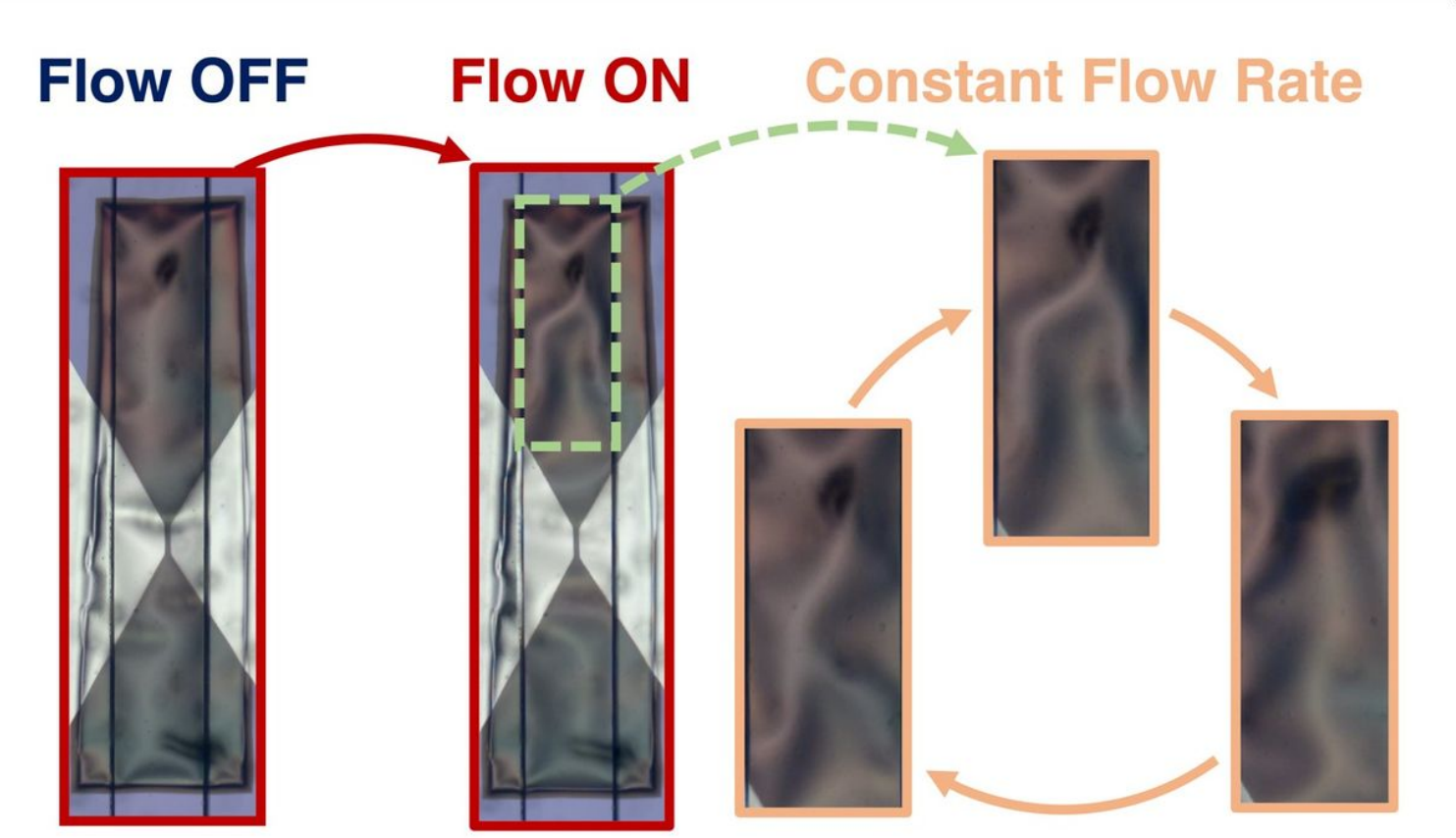

Figure 4

Periodic deformations of the membrane under constant fluid pressure. The upper part of the membrane shuttles between different deformations states (full membrane motion can be seen in the Supplementary Video 2). The duration of these transitions depended on the fluid flow inside the microchannel. The membrane dimensions are 1.5 mm length, 0.3 mm width, 220 nm thickness.

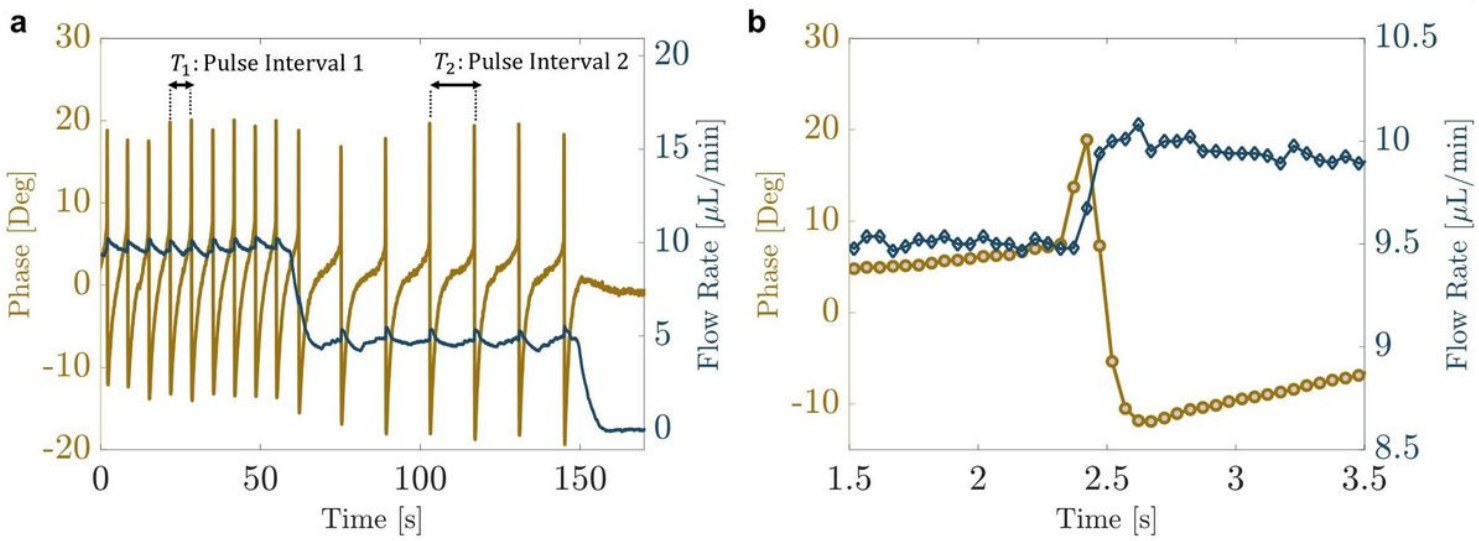

Figure 5

(a) An example time-trace of the pulsation behavior of the sensor. The microwave response and the flow rate obtained from the reference flow sensor were measured and recorded simultaneously by LabVIEW. The pulsation periods depended on the set flow rate. (b) Close up view of an event sequence. First, the membrane starts to deflect inducing a change in the phase of the microwave sensor (dark yellow trace), and then a follow-up perturbation occurred in the commercial flow rate sensor (dark blue trace).

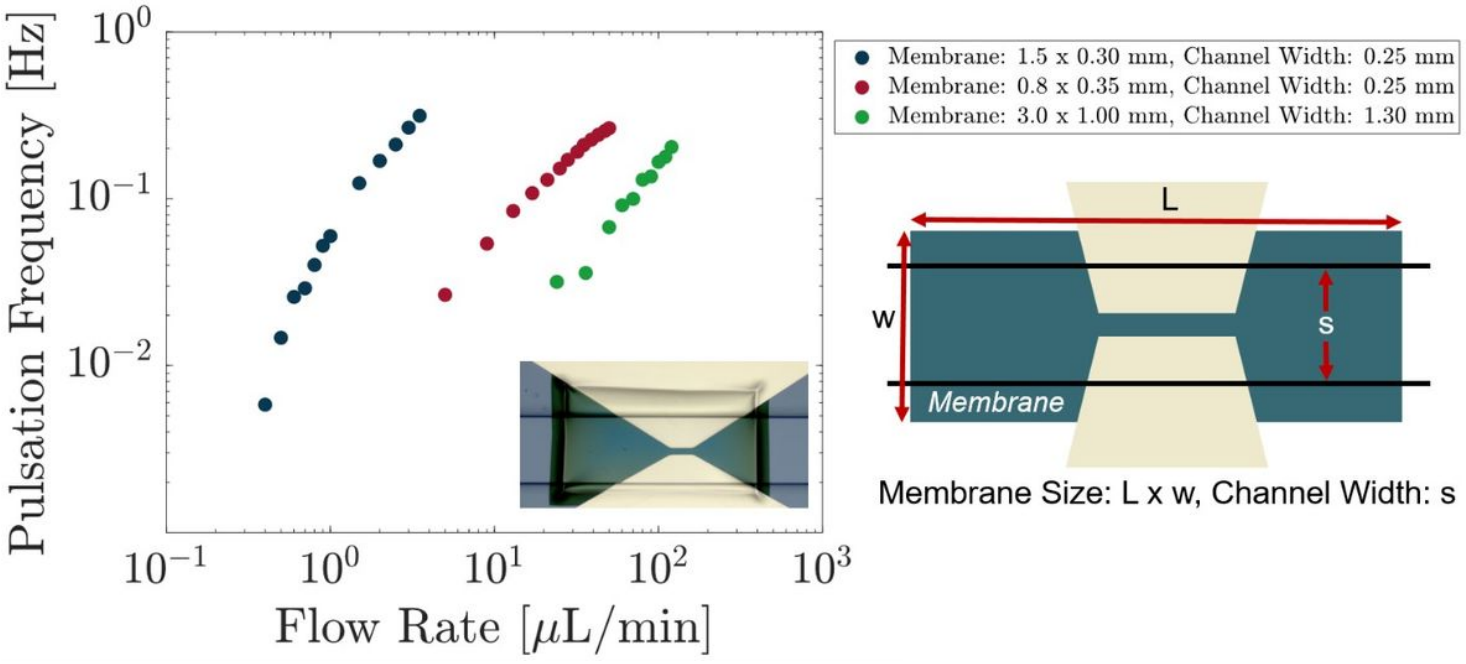

Figure 6

Pulsation frequency as a function of flow rates for different geometries. Three different devices were used in the experiments and their dimensions are provided. In all three experiments, pulsation frequencies were observed to increase monotonically, as the flow rate was increased.

Supplementary Files

This is a list of supplementary files associated with this preprint. Click to download.

- FlowSensorSI.pdf
- SupplementaryVideo1.mp4
- SupplementaryVideo2.mp4